

MOLYBDENUM (IV) SULFIDE-GRAPHENE (MO₂-RGO) MEMBRANES SUPPORTED ONTO ALUMINA SUBSTRATES FOR BPA REMOVAL

Faizatul Syazwani Zulkifili, Dr Sherif AbdulBari Ali, Dr Nur Hidayati Othman,

Faculty of Chemical Engineering, Universiti Teknologi MARA

Abstract— Graphene oxide (GO) is an example of graphene derivatives composed of carbon atoms that are bonded by van der Waals forces and have intriguing characteristics such as single atomic layer thickness, high mechanical strength and large specific surface area. GO membranes have been widely used for water treatment and electronic applications. Removal of endocrine disrupting compounds such as BPA into the water system can cause harmful effects to the environment and membrane separation is found as one of the cost efficient in removing BPA. In this study, adsorption of BPA by using molybdenum disulfide-reduced graphene oxide (MoS₂-rGO) as adsorbent supported onto alumina has been made. Simple physical method has been used in synthesizing MoS₂ and rGO by exfoliation and modified Hummer's method respectively. The composite membrane were characterized under scanning electron microscope (SEM), field scanning electron microscope (FESEM), mercury porosimeter (Hg Porosimetry), atomic force microscope (AFM), digital microscope and contact angle while UV-Vis for BPA rejection. The effects of pressure found that higher pressure resulted the better separation and after 120 ppm the performance of membrane decrease due to fouling. MoS₂-rGO/alumina membrane exerts the best BPA rejection at 120 ppm and 1.5 bar with 63.18% rate.

Keywords — molybdenum disulfide, reduced graphene oxide, alumina, BPA

I. INTRODUCTION

Water pollution has become the most serious problem in the entire world as the polluted water may contain heavy metals such as chromium (Cr), copper (Cu), lead (Pb) and organic pollutants such as dye which is mostly used in textile industries [1-2]. According to Petrie, BPA is frequently found in the environment including surface waters [3]. Other than the organic contaminants, many techniques have been applied in treating waste water which are adsorption, photocatalytic degradation and chemical oxidation[4].

BPA is an abbreviation used for bisphenol A, a chemical that is being used in the manufacturing of plastics and resins and it is a colourless solid that is soluble in organic solvent but poorly soluble in water [5]. The conventional technique in treating BPA is by biological treatment method. BPA treatment however possess many problems with the conventional technology which are it is ineffective and the regeneration is expensive hence will result in loss of the adsorbent leading to higher cost [6] in treating the organic contaminants. Suspended solid concentrations in the effluent is particularly high is subjected to the problem with conventional technology in treating BPA. The current technology used to treat BPA is through electrochemical oxidation but the effectiveness is not really assured. This method is depending on the properties of anodes and the organic contaminants to be removed. For instance, graphite is the traditional electrodes used for wastewater treatment and it is observed that the performance in wastewater is low[7].

Membrane is used as an alternative to remove BPA as membrane technology can be reliable, do not harm the environment where no generation of secondary products, ease of operation, low cost and has low energy consumption [8]. It has low energy consumption because there is no phase change occurs throughout the process [9]. Despite of the advantages, membrane separation is exposed to some disadvantages of having membrane fouling and deterioration. Fouling happens when there is a deposition on the surface of the membrane and has the tendency to reduce the permeate flux. This phenomena could reduce the separation and membrane lifespan leading to the increment of energy as higher feed pressure is required, hence increase the capital cost [10]. Ceramic membrane is used as the substitute to membrane and it is the best choice apart from the synthetic membrane. Alumina is one of the ceramic membrane commonly adapted to wastewater treatment as it shows excellent performance in harsh conditions, high filtration flux, long service life and ease of cleaning [11].

Graphene is a one-atomic layer of carbon atoms that is arranged in honeycomb lattice [12] and it was known to be 200 times stronger than steel even it is the thinnest material in nature [13]. Besides of its strength, graphene is also an excellent conductor of heat and electricity as well as has high light absorption abilities. Because of the incredibly amazing features, graphene has been used in various applications such as liquid crystal display (LCD), photovoltaic cells and computer chips. Graphene oxide is characterized by a distinctive structure of carbon, oxygen and hydrogen in a given ratios. In graphene oxide, the carbon atoms covalently bonded to oxygen functional groups such as hydroxyl [13]. Graphene oxide is has its own uniqueness in terms of ease dispersibility in water and organic solvents which will ease the combination process of graphene oxide with ceramic membranes. Graphene oxide can be synthesized using Hummer's method by oxidizing the natural flake graphite. rGO is actually an abbreviation to reduced graphene oxide and is obtained after further reduction of graphene oxide. It can be produced in large quantities also has excellent electrical conductivity. Other than that, the low cost of rGO is the reason why rGO is been widely used in industry. Due to the presence of oxygen functionalities of graphene oxide, it can easily disperse in organic solvents and water. This creates a major advantages when combining with ceramic membranes to increase their electrical and mechanical properties [14].

Molybdenum disulfide (MoS₂) is made up of a single atomic layer of molybdenum and two single layer of sulfur and it is relatively unreactive to dilute acids and oxygen. Advantages of MoS₂ are it is stable in aqueous solution, has frictionless smooth surface, antifouling and has photocatalytic function. The limitations exert on MoS₂ is it exhibits high permeance but has low gas selectivity. In relation to membrane separation, it is found that thicker membrane will results in lower mass transfer coefficient and poor permeability hence MoS₂ is used as it can improves permeability in removing BPA [15].

Alumina is a white granular material and one of the most important ceramic materials used as adsorbent for removal of dissolved organic contaminants from waste water. Alumina is also

known as one of the most active adsorbent used to remove heavy metal ions. Alumina is being used as substrates because it can resist strong alkali and acid attack at elevated temperature, good thermal conductivity and has high strength [16]. Alumina or aluminium oxide possess strong ionic inter-atomic bonding giving its rise in desirable characteristics and it exists in several crystalline phases such as alpha phase alumina. Alpha phase alumina exerts the strongest and stiffest of the oxide ceramics.

The coating of MoS₂-rGO onto alumina can further enhance the removal of BPA in wastewater as they can be fabricated into thin films with high chemical robustness. By doing this method, the overall cost in treating BPA in wastewater can be reduced

II..METHODOLOGY

A. Materials

Flake graphite powder (99% purity), BPA granules were obtained from Sigma-Aldrich. Hydrochloric acid (HCl, 95%), hydrogen peroxide (H₂O₂, 30%), potassium permanganate (KMnO₄, MW 158.03g), ammonia (NH₃) were of the same brand of R&M Chemicals. Sulphuric acid (H₂SO₄, 98%), sodium nitrate (NaNO₃, 99%), L-ascorbic acid (C₆H₈O₆, 99%) and acetone (C₃H₆O) were all of System brand and were used as received. Deionized water from Millipore system was used.

B. Synthesis of MoS₂

0.25 g of dried MoS₂ was reacted in 100 mL isopropanol. The mixture was then sonicated for 4 hours and left the mixture overnight for sedimentation. The bottom layer of the sediment was dried in an oven at 70°C for 24 hours [17].

C. Synthesis of GO by Modified Hummer's method

Graphene oxide was synthesized using modified hummer's method [18]. 10 g of graphite powder, 5 g of sodium nitrate and 400 mL of concentrated H₂SO₄ were mixed in an ice bath condition under 15°C. 15 g of KMnO₄ was added gradually in 2 hours and this mixture was stirred for 20 hours. 200 mL of distilled water was added to increase the temperature to 70°C and 90°C respectively. The reaction was terminated by the addition of 60 mL H₂O₂. The brownish product was then washed with hydrochloric acid before being separated by centrifugation under 10000 rpm for 30 minutes. The slurry product being washed with acetone and dried under 70°C overnight.

D. Synthesis of rGO

Graphene oxide was reduced by L-ascorbic acid to produce reduced graphene oxide. 1.5 g of graphene oxide was mixed in 500 mL of deionized water and stirred for 30 min. The mixture was sonicated for 2 hours before 15 g of ascorbic acid was added. It was then stirred for 30 min and 25 g of ammonia solution was added until pH 9.5 was reached. The mixture was then heated to 95°C and continuously stirred for 2 hours. The resultant black precipitate was filtered with vacuum pump and further washed with simultaneous distilled water and acetone. The filtered precipitate was dried in oven overnight.

E. Synthesis of MoS₂-rGO

0.1 g of MoS₂ and rGO were mixed in 100 mL beaker. The mixture was sonicated for 1 hour at room temperature to obtain a perfectly mixed suspension.

F. Coating of MoS₂-rGO onto alumina

MoS₂-rGO was coated onto alumina via simple vacuum filtration method (Fig.1). This coating was done because the deposition of MoS₂-rGO can further increase the performance of alumina in rejecting BPA. 0.1 g MoS₂ powder and 0.1 g rGO were dispersed in 100 mL of deionized water and undergoes sonication for 60 minutes. The solution was dispersed onto alumina membrane and filtered under vacuum filtration and the composite coating of MoS₂-rGO onto alumina were dried [19].

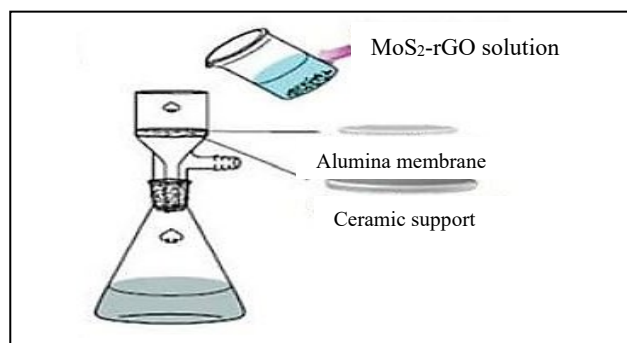


Fig. 1 Set up of membrane coating

G. Synthesis of BPA stock solution

1 g of BPA granules were mixed in 2L distilled water in order to prepare 500ppm solution. 10mL of ethanol was added to the solution. The solution was further diluted with distilled water to 100, 120 and 140 ppm.

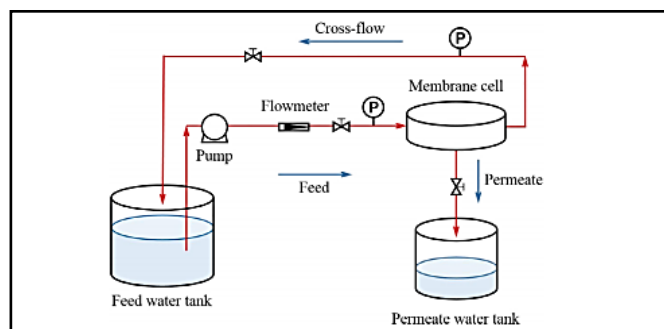
H. Pure Water Flux

In order to investigate the filtration performance of the samples, the membranes were used to determine the pure water flux (PWF) at a trans-membrane pressure [20] of 1.5, 1.0 and 0.5 bar. The cross flow set up of membrane filtration can be seen in Fig 2. PWF was calculated as in Equation 1:

$$J = \frac{V}{A\Delta t} \quad \text{Equation 1}$$

where J is pure water flux (L/m².h), V is volume of permeate (L), A is effective membrane area (m²) and Δt is permeate time (h).

Fig. 2 Schematic diagram of membrane filtration [11]



I. BPA removal testing

In membrane testing, the concentration of BPA were varied to 100, 120 and 140 ppm. Each concentration were tested with 0.5, 1.0 and 1.5 bar pressure. To evaluate the performance of membrane, dead-end dynamic adsorption operation was used where the flow is passed tangential to the membrane[21]. Membrane filtration set up can be seen in Fig. 2.

J. BPA rejection flux

BPA rejection flux can was done after the BPA testing. The rate of BPA rejection characterized by UV-VIS can be calculated using Equation 2 where R is rejection rate (%), C_p is concentration permeate (g/L) and C_f is concentration feed solution (g/L).

$$R = \left(1 - \frac{C_p}{C_f}\right) \quad \text{Equation 2}$$

K. Characterization

Wide angle (10° - 80° , 45 kV/20 mA) powder X-Ray diffraction (XRD) was conducted using X-Ray Diffractometer (PANalytical, X'Pert Pro) to observe the crystal phase of the as-prepared nanocomposites and MoS₂ precursor. Fourier Transform Infrared (FTIR) Spectra (Perkin Elmer, FTIR Spectrum One) was used to analyze the functional groups of nanostructures in 400-4000 cm⁻¹ wavelength. The thermal stability of MoS₂ and MoS₂-rGO nanocomposite was studied by thermogravimetric analyses (TGA, TGA851/1600) in nitrogen atmosphere, temperature range of 25°C-1000°C and heating rate of 10°C/min. Pore size distribution analysis of membranes can be performed by Mercury Porosimeter (Micromeritics Auto Pore IV). Three dimensional surface structures of MoS₂-rGO on alumina was analyzed with atomic force microscopy (AFM, Park XE-100). Cross section of the prepared membrane was characterized by digital microscope (Daniu LED 500X 2MP). The microstructure of nanofillers were studied by Field Scanning Electron Microscopy (FESEM, Hitachi Backscatter Detector S-3000). Cross section of membranes was examined under 500-5000 magnification. Hydrophilicity of bare alumina and MoS₂-rGO nanocomposites can be analyzed with Sessile drop technique utilizing VCA 3000S Water Surface Analysis System.

III. RESULTS AND DISCUSSION

A. Characterization of synthesized powder

a. Functional group

Fig. 3 shows the Fourier Transform Infrared (FTIR) spectra for graphite, graphene oxide and reduced graphene oxide where it is used to investigate the presence of functional group in each sample. The mechanism of FTIR is based on the vibrational excitation of molecular bonds by adsorbing infrared light energy within wavelength of 500 cm⁻¹ to 4000 cm⁻¹ [22] Initially, graphene oxide is expected to have more oxygen containing functional group as it has been exposed to strong oxidants under oxidation process from graphite [23]. It can be seen from Fig. 3 that graphite has no significant peak while for graphene oxide, it has a broader peak as compared to reduced graphene oxide. Fig. 3 shows various peaks that are related to their respective functional groups. First and foremost, O-H stretching has occurred at 3547 cm⁻¹, C=O stretching at 1750 cm⁻¹, O-H deformation at 1325 cm⁻¹ and C-O stretching at 1116 cm⁻¹ were clearly observed in the spectrum of GO. The highest peak of GO at 3457 cm⁻¹ indicates to the attribution of water

molecules [1]. With the presence of all these carboxylic, hydroxyl, epoxide and carbonyl groups, oxygen molecules were confirmed to be greatly occupied at the edge and basal plane of GO which can be concluded that GO was synthesized successfully [24]. For rGO, the intensities of the bands associated with the oxygen functional groups strongly decreased in relation to those of GO [1]. rGO which can be obtained by reduction of graphene oxide is expected to have a lower amount of oxygen containing functional group. As shown in the graph, the broad peak at 3547 cm⁻¹ has disappeared which reveals the absence of hydroxyl functional group [25]. Peak at 1116 cm⁻¹ became less intense than those peaks at the same location in FTIR spectra of GO, which were also due to the removal oxygen by using L. ascorbic acid during the reduction. Therefore, the oxygen-containing functional groups are successfully removed partially and the low amounts of residue of functional groups are still remain at the edge and basal plane of rGO[26].

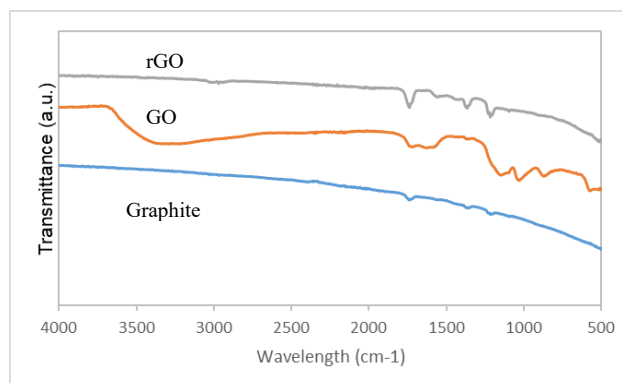


Fig. 3 FTIR spectra of graphite, GO and rGO

The spectra of rGO-MoS₂ and MoS₂-rGO (Fig. 4) displayed that rGO have adsorption peaks at 1736, 1551, 1417, 1366 and 1215 cm⁻¹ which were assigned to the C=O, C=C, C-O, C-OH and C-O groups respectively. The decrease in peak intensity of the oxygen-rich functional group present in MoS₂-rGO suggested the successful reduction of GO to rGO. Moreover, the peak concentrated at 609 cm⁻¹ of MoS₂ correspond to Mo-S vibration [27].

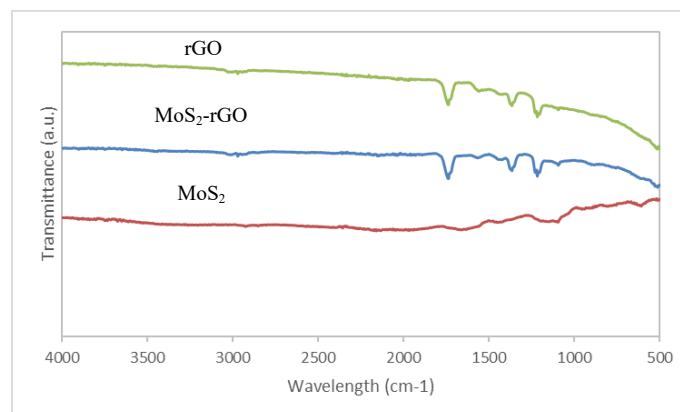


Fig. 4 FTIR spectra of MoS₂, rGO and MoS₂-rGO

b. Crystallization of graphite, GO and rGO

Fig. 5 shows the X-ray diffraction image of graphite, GO and rGO. It can be seen that natural graphite powder presented a basal reflection peak at $2\theta = 26.44^\circ$ [28]. The increment in interlayer spacing of GO in Figure 5b results the peak to be shifted to $2\theta = 10.81^\circ$ which indicates the incorporation of oxygen functional groups in graphite. An increase in interlayer spacing is mainly attributed to the intercalation with water and the presence of oxygen functionalities such hydroxyl groups which populate on the basal plane of the carbon sheet[29]. After the reduction of GO to rGO in Fig. 5 with the removal of oxygen functional group, the interlayer

spacing seems to decrease and the peak shifted to $2\theta = 25.50$ [30]. The crystal phase of the as prepared nanocomposites and MoS_2 precursor was analyzed under XRD and the data were presented in Fig 6. MoS_2 showed diffraction peaks at 14° , 32° and 57° which indicated that the layered MoS_2 having lamellar structure [31]. Bulk MoS_2 possess the highest peak at 14° indicates that the sample is implicative of a highly exfoliated nature [32]. MoS_2 -rGO nanocomposites displays the same peak as pure MoS_2 , the peak characteristics diffraction rate of MoS_2 -rGO is at $\theta = 27^\circ$. This diffraction confirms the presence of rGO in the nanocomposites [31].

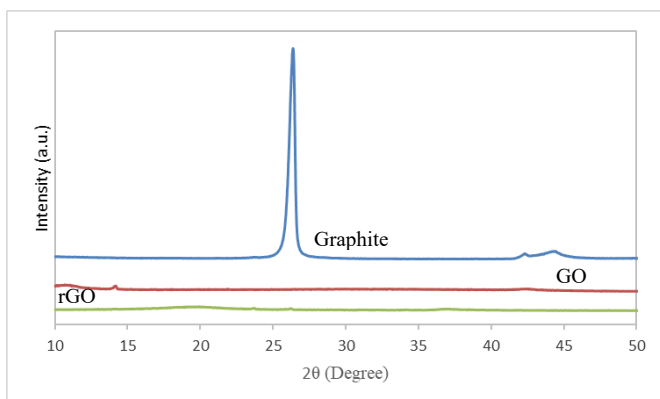


Fig. 5 XRD images of graphite, GO and rGO

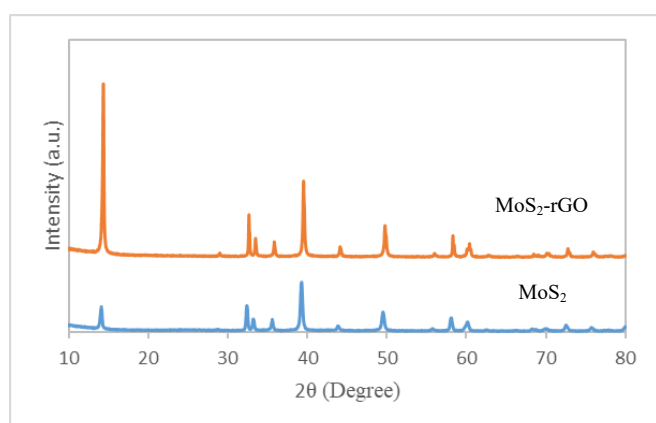


Fig. 6 XRD pattern of bulk MoS_2 and MoS_2 -rGO

c. Thermal stability

The thermal stability of GO, rGO, pure MoS_2 and exfoliated MoS_2 , the sample was tested with TGA851/1600 and the TGA curves of are shown in Fig. 7 and Fig. 8 respectively. GO in Fig.7 showed initial weight loss at 100°C and this happens because of the presence of moisture and it exhibited 20% weight loss between 170°C and 350°C owing to the removal of oxygen functional group in the form of carbon dioxide and carbon monoxide. The weight loss of rGO is lower than that of GO particularly in the range of 240°C and 420°C which is clear indication of the decrease in the oxygen functionalities by means of profound reduction of GO[33]. Bulk MoS_2 showed relatively high thermal stability and the weight loss is about 1% at 950°C while exfoliated MoS_2 (Fig. 8b) has higher thermal stability than pure MoS_2 [34].

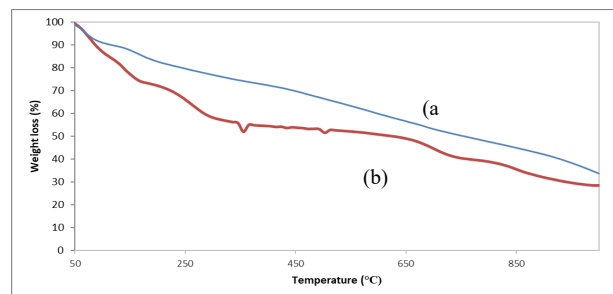


Fig. 7 TGA diagram of (a) GO and (b) rGO

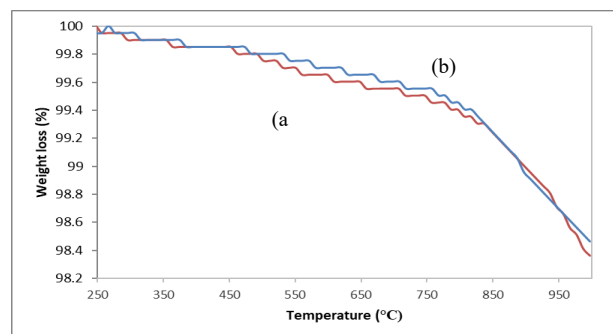


Fig. 8 TGA diagram of (a) pure MoS_2 (b) exfoliated MoS_2

B. Characterization of synthesized membrane

a. Hydrophilicity

Hydrophilicity is one of the vital characteristic for water permeance testing[35]. Contact angle is basically an angle that a liquid creates with solid surface of a porous material when both of the materials come in contact. This angle is determined by both properties of the solid and liquid also the interaction and repulsion forces between liquid and solid. Cohesion and adhesion forces are the interactions involved where cohesion forces acted on similar molecules of liquid while adhesive forces acted on dissimilar molecules. These forces will determine the contact angle created in the solid and liquid interface[36]. Small contact angles ($< 90^\circ$) correspond to high wettability, while large contact angles ($> 90^\circ$) correspond to low wettability[37]. The contact angle for bare alumina gives a value of 20.30° (Fig. 9a). This indicates that it has a small contact angle which means the cohesive forces are weaker than the adhesive forces resulting in molecules of liquid to interact with the solid molecules. The contact angle of composites coatings of MoS_2 -rGO onto alumina is shown in Fig. 9b. The liquid used during the testing is liquid water resulting in surface tension of 36.98 and contact angle of 77.80° . A low contact angle which denoted less than 90° indicates that the surface is high wetting which means that the water droplet spreads out more on the surface of composite coating. High wetting results in the strong attractive forces in pulling the liquid droplet down causing it to spread out. Low contact angle will cause the surface energy to increase thus having high interfacial tension[36]. Low contact angle also indicates that the membrane has small pores and increase the efficiency in removing BPA.

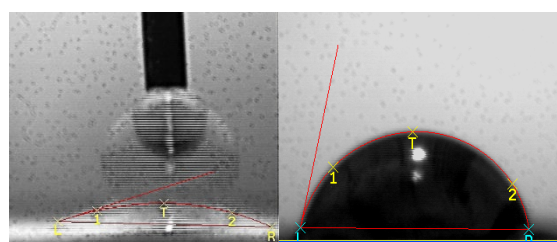


Fig. 9 (a) Bare alumina, (b) MoS_2 -rGO on alumina

b. Morphology

The pore size distribution of bare alumina was determined with a mercury porosimeter and the results were given in Fig. 10 (a,b). It can be seen that the pore diameter of bare alumina has the highest peak at 89.33 μm while for MoS₂-rGO/alumina is at 6.03 μm[38]. The increase in pore diameter is the result from the unique core-shell alumina with improved porosity hence produce strong interaction[39]. Fig. 10b indicates that the surface of alumina has been closed by the coating hence the pore volume decreased.

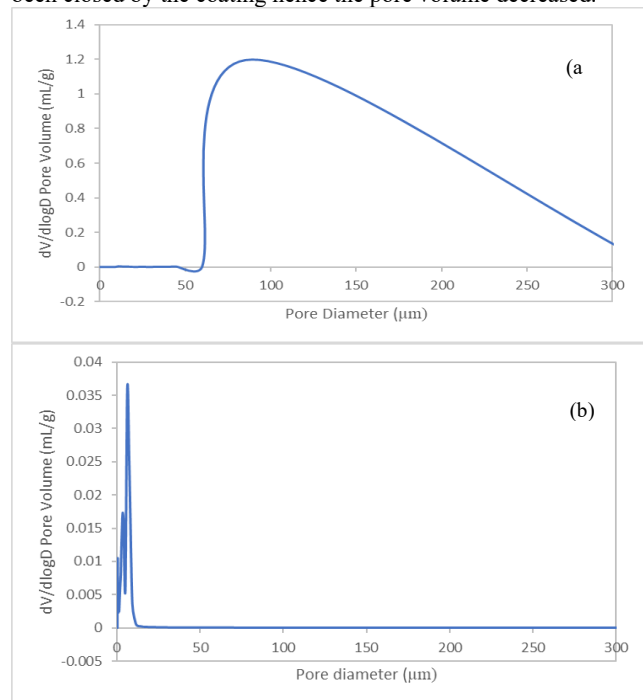


Fig. 10 Pore size distribution of (a) bare alumina and (b) MoS₂-rGO/alumina

The two and three-dimensional surface morphologies of the bare alumina support was characterized by AFM. The surface structures for the membranes are shown in Fig. 11. The obtained root-mean squared roughness (Rq) which provides an indicator of surface roughness revealed changes in surface morphology upon the growth of MoS₂-rGO nanostructures on the membrane. The formation of MoS₂-rGO onto alumina resulted in increased Rq value because of the increased surface coverage by larger amount of MoS₂-rGO nanostructures on the membrane[40]. MoS₂-rGO membrane has a rougher surface compared to bare alumina as indicated by Rq roughness value [41]. The Rq of bare alumina and MoS₂-rGO membrane is represented in Table 3.1.

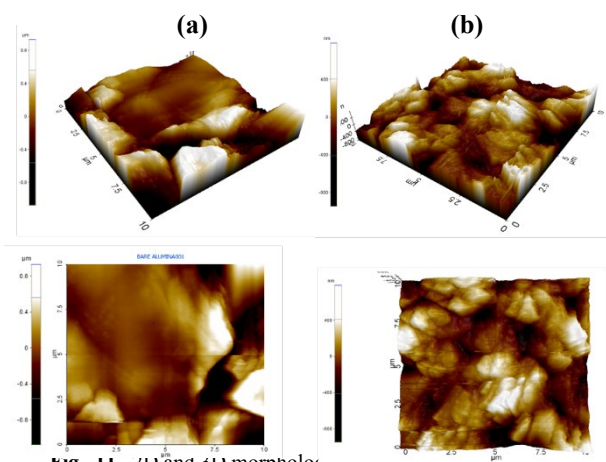


Fig. 11 2D and 3D morphology of (a) bare alumina and (b) MoS₂-rGO membrane

Table 1 Roughness of membranes

Sample	Root mean squared roughness (Rq)
Bare alumina	286.497
MoS ₂ -rGO membrane	707.562

Surface morphology can also be identified by using digital microscope. Fig. 12a below showed the pore structure of bare alumina where it can be seen that it has a porous structure hence allowing it to be used in membrane filtration. The coating of MoS₂-rGO onto alumina membrane had resulted in the adsorption on the surface of the membrane. The diagram of MoS₂-rGO coating was illustrated in Fig. 12b.

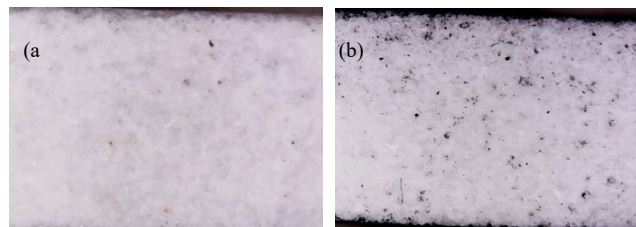


Fig. 12 Digital microscopy of (a) bare alumina (b) MoS₂-rGO onto alumina

The surface of nanostructures MoS₂-rGO on the support were characterized with FESEM (Fig. 13). As shown in Fig 13a and b, the bare alumina membrane as a macro porous support was composed of large Al₂O₃ particle with an irregular size and shape [40]. The FESEM image of MoS₂-rGO (Fig 13 c,d) illustrates a 3D sphere-like architecture and the overlapping of graphene layers is caused by the interaction of MoS₂ and rGO. This resulted in high specific surface area which helps in adsorption and contribute to the stability of MoS₂-rGO[42].

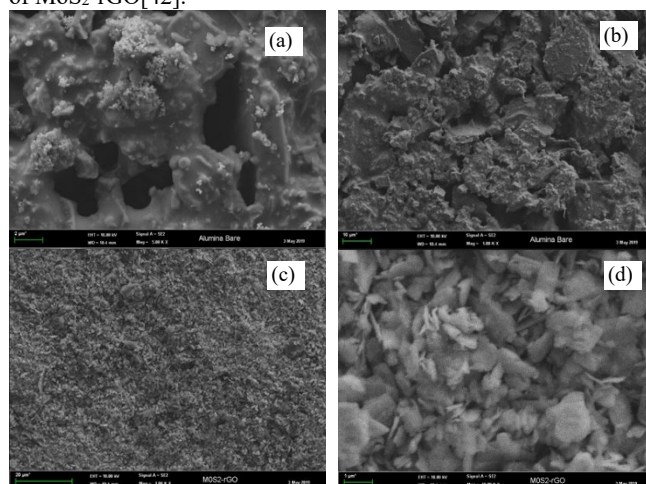


Fig. 13 FESEM image of (a,b) bare alumina and (c,d) MoS₂-rGO coated Membrane surfaces

c. Pure Water flux

Pure water flux was done to compare the performance of bare alumina and MoS₂-rGO membrane (Fig 15) in transporting water through the membrane pores. The inversely proportional relationship resulted in the lower pure water flux over time. It can be seen that bare alumina with the highest pressure obtained the highest pure water flux of 3973 L/m².h while MoS₂-rGO membrane has a slight decrement in pure water flux at the same pressure. This may be caused by the hindrance of the coating material on the surface of the membrane that resulted in lower membrane performance (2975 L/m².h) in transporting water. Both bare alumina (1300 L/m².h) and coated membranes (1131 L/m².h) have the least

pure water flux at 0.5 bar were because of insufficient supply of energy hence low flow rate travelled on the membrane surface. Bare alumina at 1.0 bar was decreasing in pure water flux over 60 minutes but MoS₂-rGO membrane was having a very low water flux. The reason for the non-decreasing pure water flux was a slight increment in the pressure while conducting the test hence more volume were collected as compared to bare alumina.

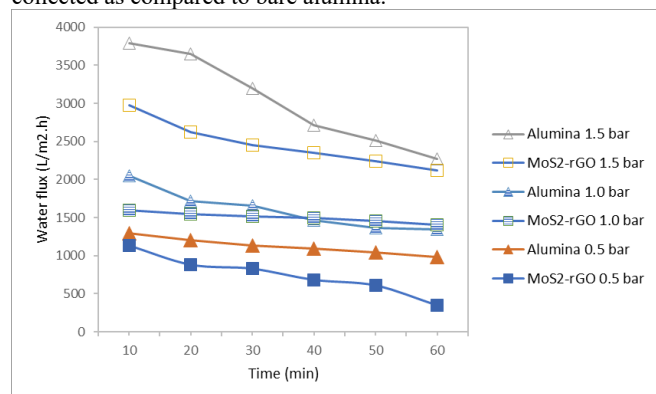


Fig 15 Pure water flux of alumina and coated membranes at different pressure

d. BPA rejection using UV-VIS

The volatility and thermal stability presented by BPA make it suitable for detection using spectrophotometer[43]. The amount of BPA rejected from the sample was determined from calibration curve that was set as a standard curve. The calibration curve was shown in Fig 16 was nearly linear with value of R² of 0.994 range from 60 to 200ppm. The highest absorbance for 100, 120 and 140ppm were 0.0411, 0.0564 and 0.0667 respectively.

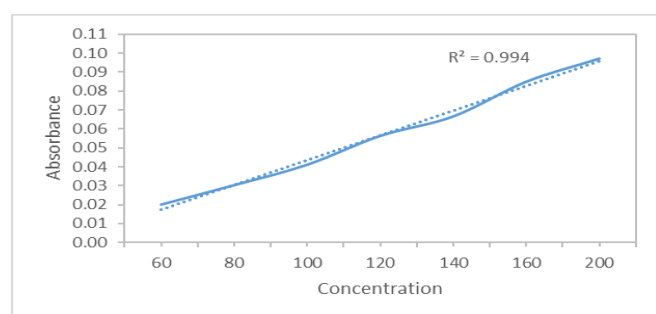


Fig 16 Calibration curve for BPA

BPA rejection for all concentrations can be illustrated in Fig 17 where MoS₂-rGO membrane has the highest performance when 1.5 bar pressure was applied. From the figure, 1.5 bar exerted the highest rejection rate of 63.18% while 0.5 bar has the lowest rejection rate of 37.32% at 120 ppm. This happened because the rejection efficiency declined with the increase of BPA concentration. The greater removal of BPA seen in 1.5 bar is because higher pressure capable in increasing the rate of water flow through the membrane hence lowered the BPA concentration in the permeate. BPA removal with 0.5 bar increased to 37.32% because it was expected that some of the BPA present in the permeate. It can be seen that after 120ppm, the rejection of BPA has decreased about half from 120 ppm due to the fouling of the membrane.

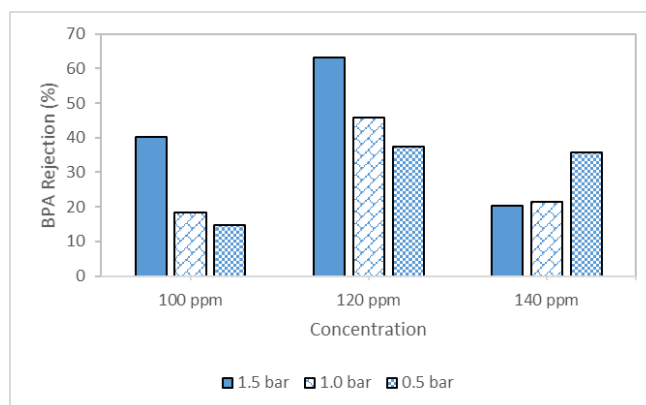


Fig 17 Rejection of BPA with various conditions

IV. CONCLUSION

In summary, the composites of GO and rGO with the MoS₂ have been synthesized and its use is known to be environmentally safe. A novel MoS₂-rGO supported onto alumina membrane was prepared through coagglomeration of MoS₂ and rGO in deionized water. Those parameters including feed concentration and pressure affect the rejection of BPA. The higher the pressure, the better the separation of BPA and further removal of BPA at 140 ppm has a decrement in performance. Further work is necessary to focus on reducing the thickness of coating layer to improve the water permeance and this kind of ceramic membrane can be a promising material in electronic application.

ACKNOWLEDGMENT

Thank you to Dr. Syerif Abdulbari Ali and Dr. Nur Hidayati Othman as well as Universiti Teknologi MARA

References

- [1] G. S., H. J.W., E. V., and K. J.-H., "Biocompatibility of microbially reduced graphene oxide in primary mouse embryonic fibroblast cells," *Colloids Surfaces B Biointerfaces*, vol. 105, pp. 58–66, 2013.
- [2] H. Nicholas, J. Hoong, and N. Ismail, "Removal of Dye in Wastewater by Adsorption- Coagulation Combined System with Hibiscus sabdariffa as the Coagulant," vol. 01008, 2018.
- [3] B. Petrie, L. Lopardo, K. Proctor, J. Youdan, R. Barden, and B. Kasprzyk-Hordern, "Assessment of bisphenol-A in the urban water cycle," *Sci. Total Environ.*, vol. 650, pp. 900–907, 2019.
- [4] M. hong Wu, L. Li, N. Liu, D. jin Wang, Y. cheng Xue, and L. Tang, "Molybdenum disulfide (MoS₂) as a co-catalyst for photocatalytic degradation of organic contaminants: A review," *Process Saf. Environ. Prot.*, vol. 118, pp. 40–58, 2018.
- [5] N. Singh, "Exposure to Bisphenol-A Through Excess Use of Polymer , With Environmental Toxicity," vol. 2, no. 3, pp. 454–457, 2016.
- [6] G. Z. Kyzas, J. Fu, and K. A. Matis, "The change from past to future for adsorbent materials in treatment of dyeing wastewaters," *Materials (Basel)*, vol. 6, no. 11, pp. 5131–5158, 2013.
- [7] C. W. Yang, "Degradation of bisphenol A using electrochemical assistant Fe(II)-activated peroxydisulfate process," *Water Sci. Eng.*, vol. 8, no. 2, pp. 139–144, 2015.
- [8] S. I. Siddiqui and S. A. Chaudhry, "A review on graphene oxide and its composites preparation and their use for the removal of As³⁺ and As⁵⁺ from water under the effect of various parameters: Application of isotherm, kinetic and thermodynamics," *Process Saf. Environ. Prot.*, vol. 119,

- pp. 138–163, 2018.
- [9] M. Maldovan, “Breaking separation limits in membrane technology,” *J. Memb. Sci.*, vol. 566, no. April, pp. 301–306, 2018.
- [10] M. Qasim, N. N. Darwish, S. Mhiyo, N. A. Darwish, and N. Hilal, “The use of ultrasound to mitigate membrane fouling in desalination and water treatment,” *Desalination*, vol. 443, no. June, pp. 143–164, 2018.
- [11] Y. Zhu *et al.*, “Fabrication of composite membrane with adsorption property and its application to the removal of endocrine disrupting compounds during filtration process,” *Chem. Eng. J.*, vol. 352, pp. 53–63, 2018.
- [12] F. Mark, O. Goerbig, and L. Notes, “Introduction to the Physical Properties of Graphene,” 2008.
- [13] L. De Marchi, C. Pretti, B. Gabriel, P. A. A. P. Marques, R. Freitas, and V. Neto, “An overview of graphene materials: Properties, applications and toxicity on aquatic environments,” *Sci. Total Environ.*, vol. 631–632, pp. 1440–1456, 2018.
- [14] H. Ahmad, M. Fan, and D. Hui, “Graphene oxide incorporated functional materials: A review,” *Compos. Part B*, 2018.
- [15] Y. Ma *et al.*, “Study of the effect of membrane thickness on microcapsule strength, permeability, and cell proliferation,” pp. 1–9, 2012.
- [16] Z. Hao, B. Wu, and T. Wu, “Preparation of alumina ceramic by κ -Al₂O₃,” *Ceram. Int.*, vol. 44, no. 7, pp. 7963–7966, 2018.
- [17] W. Zhang, P. Zhang, Z. Su, and G. Wei, “Synthesis and sensor applications of MoS₂-based nanocomposites,” *Nanoscale*, vol. 7, no. 44, pp. 18364–18378, 2015.
- [18] N. I. Zaaba, K. L. Foo, U. Hashim, S. J. Tan, W. W. Liu, and C. H. Voon, “Synthesis of Graphene Oxide using Modified Hummers Method: Solvent Influence,” *Procedia Eng.*, vol. 184, pp. 469–477, 2017.
- [19] M. Cheng, L. Huang, Y. Wang, and J. Tang, “RSC Advances nanometal composite filter membranes,” pp. 47886–47897, 2017.
- [20] B. Jaleh, N. Gavar, P. Fakhri, N. Muensit, and S. M. Taheri, “Characteristics of PVDF membranes irradiated by electron beam,” *Membranes (Basel)*, vol. 5, no. 1, pp. 1–10, 2015.
- [21] A. Onur, A. Ng, W. Batchelor, and G. Garnier, “Multi-Layer Filters: Adsorption and Filtration Mechanisms for Improved Separation,” vol. 6, no. September, pp. 1–11, 2018.
- [22] M. Bera, Chandravati, P. Gupta, and P. K. Maji, “Facile One-Pot Synthesis of Graphene Oxide by Sonication Assisted Mechanochemical Approach and Its Surface Chemistry,” *J. Nanosci. Nanotechnol.*, vol. 18, no. 2, pp. 902–912, 2017.
- [23] A. Ibarra-Hernández, A. Vega-Rios, and V. Osuna, “Synthesis of Graphite Oxide with Different Surface Oxygen Contents Assisted Microwave Radiation,” *Nanomaterials*, vol. 8, no. 2, p. 106, 2018.
- [24] N. M. S. Hidayah *et al.*, “Comparison on graphite, graphene oxide and reduced graphene oxide: Synthesis and characterization,” *AIP Conf. Proc.*, vol. 1892, 2017.
- [25] Y. Gong, D. Li, Q. Fu, and C. Pan, “Influence of graphene microstructures on electrochemical performance for supercapacitors,” *Prog. Nat. Sci. Mater. Int.*, vol. 25, no. 5, pp. 379–385, 2015.
- [26] J. Ma, D. Ping, and X. Dong, “Recent Developments of Graphene Oxide-Based Membranes: A Review,” 2017.
- [27] R. Vinoth *et al.*, “Synergistically Enhanced Electrocatalytic Performance of an N-Doped Graphene Quantum Dot-Decorated 3D MoS₂-Graphene Nanohybrid for Oxygen Reduction Reaction,” *ACS Omega*, vol. 1, no. 5, pp. 971–980, 2016.
- [28] Y. Chen *et al.*, “Microbial reduction of graphene oxide by *Azotobacter chroococcum*,” *Chem. Phys. Lett.*, vol. 677, pp. 143–147, 2017.
- [29] H. H. Huang, K. K. H. De Silva, G. R. A. Kumara, and M. Yoshimura, “Structural Evolution of Hydrothermally Derived Reduced Graphene Oxide,” *Sci. Rep.*, vol. 8, no. 1, pp. 2–10, 2018.
- [30] K. Sa *et al.*, “Effect of reduced graphene oxide-carbon nanotubes hybrid nanofillers in mechanical properties of polymer nanocomposites,” *IOP Conf. Ser. Mater. Sci. Eng.*, vol. 338, no. 1, 2018.
- [31] A. Bahuguna *et al.*, “Nanocomposite of MoS₂-RGO as Facile, Heterogeneous, Recyclable, and Highly Efficient Green Catalyst for One-Pot Synthesis of Indole Alkaloids,” *ACS Sustain. Chem. Eng.*, vol. 5, no. 10, pp. 8551–8567, 2017.
- [32] S. Ji *et al.*, “Exfoliated MoS₂ nanosheets as efficient catalysts for electrochemical hydrogen evolution,” *Electrochim. Acta*, vol. 109, pp. 269–275, 2013.
- [33] S. Yaragalla, R. Rajendran, J. Jose, M. A. Almaadeed, N. Kalarikkal, and S. Thomas, “Preparation and characterization of green graphene using grape seed extract for bioapplications,” *Mater. Sci. Eng. C*, vol. 65, pp. 345–353, 2016.
- [34] K. Zhou, G. Tang, R. Gao, and S. Jiang, “In situ growth of 0D silica nanospheres on 2D molybdenum disulfide nanosheets: Towards reducing fire hazards of epoxy resin,” *J. Hazard. Mater.*, vol. 344, pp. 1078–1089, 2018.
- [35] J. Zhang *et al.*, “Improved hydrophilicity, permeability, antifouling and mechanical performance of PVDF composite ultrafiltration membranes tailored by oxidized low-dimensional carbon nanomaterials,” *J. Mater. Chem. A*, vol. 1, no. 9, pp. 3101–3111, 2013.
- [36] A. Siebold, M. Nardin, J. Schultz, A. Walliser, and M. Oppliger, “Effect of dynamic contact angle on capillary rise phenomena,” *Colloids Surfaces A Physicochem. Eng. Asp.*, vol. 161, no. 1, pp. 81–87, 2000.
- [37] G. Bracco and B. Holst, *Surface science techniques*, vol. 51, no. 1, 2013.
- [38] H. Xie and X. Xiong, “Journal of Environmental Chemical Engineering A porous molybdenum disulfide and reduced graphene oxide nanocomposite (MoS₂ - rGO) with high adsorption capacity for fast and preferential adsorption towards Congo red,” *Biochem. Pharmacol.*, vol. 5, no. 1, pp. 1150–1158, 2017.
- [39] C. Guan, Y. Wang, M. Zacharias, J. Wang, and H. J. Fan, “Atomic-layer-deposition alumina induced carbon on porous NiCo_{1-x}O nanonets for enhanced pseudocapacitive and Li-ion storage performance,” *Nanotechnology*, vol. 26, no. 1, p. 14001, 2015.
- [40] Ahmad, Kim, Kim, and Kim, “Diethylene Glycol-Assisted Organized TiO₂ Nanostructures for Photocatalytic Wastewater Treatment Ceramic Membranes,” *Water*, vol. 11, no. 4, p. 750, 2019.
- [41] S. Veeramuneni, J. Drelich, J. D. Miller, G. Yamauchi, and M. R. Yalamanchili, “Effect of roughness as determined by atomic force microscopy on the wetting properties of PTFE thin films,” *Polym. Eng. Sci.*, vol. 36, no. 14, pp. 1849–1855, 2004.
- [42] X. Jiang, H. Luo, Y. Yin, and W. Zhou, “Facile synthesis of MoS₂/reduced graphene oxide composites for efficient removal of Cr(VI) from aqueous solutions,” *RSC Adv.*, vol. 7, no. 39, pp. 24149–24156, 2017.
- [43] A. Yousif Hammad, “Determination Amount of Bisphenol A in Drugs and Water Drinking Container in Khartoum State, Sudan,” *Int. J. Nutr. Food Sci.*, vol. 4, no. 6, p. 609, 2016.